Table 1 Chemical composition of the experimental Al-Si-Cu-Mg alloys measured by inductively coupled plasma atomic emission spectroscopy (ICP-AES), wt.%.

Alloys	Al	Si	Cu	Mg	Ti	Zr	Mn	Cr	Fe	Ni	V	Zn	Sr
Baseline	Rem	6.79	0.51	0.35	0.11	0.002	0.008	0.001	0.09	0.004	0.017	0.008	0.015
Zr-modified	Rem	8.59	0.79	0.37	0.12	0.14	0.008	0.001	0.10	0.004	0.010	0.010	0.017

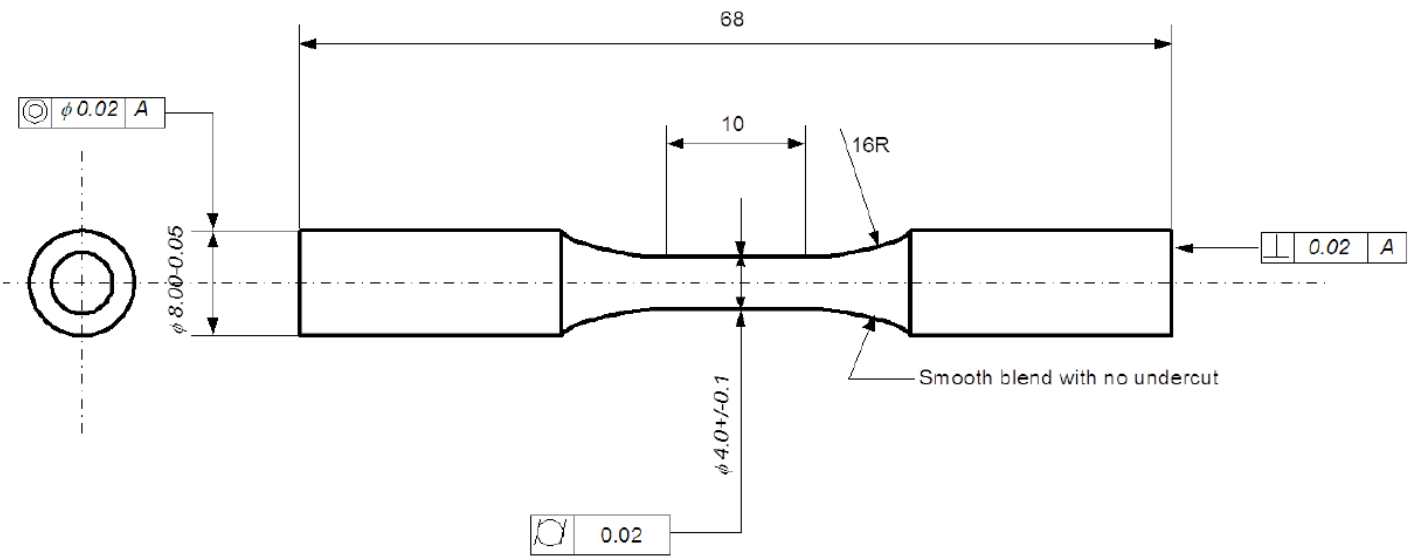

Figure 1 The geometry and dimension of the specimen subjected to the high cycle fatigue test.

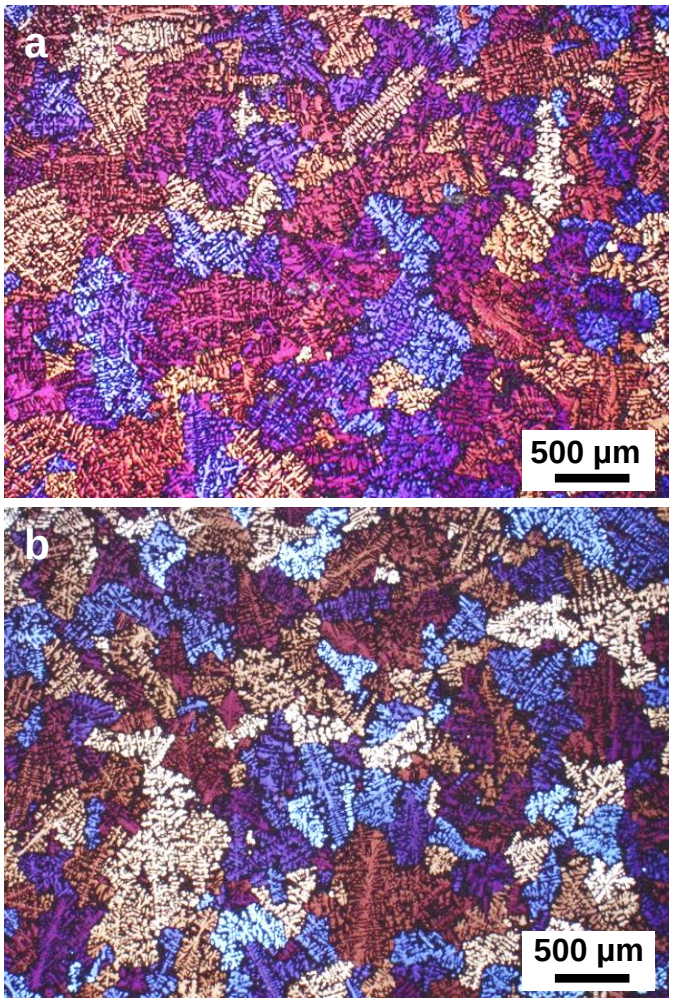

Figure 2 Optical micrographs showing the grain size of (a) baseline, and (b) Zr-modified Al-Si-Cu-Mg alloys after T6 heat treatment.

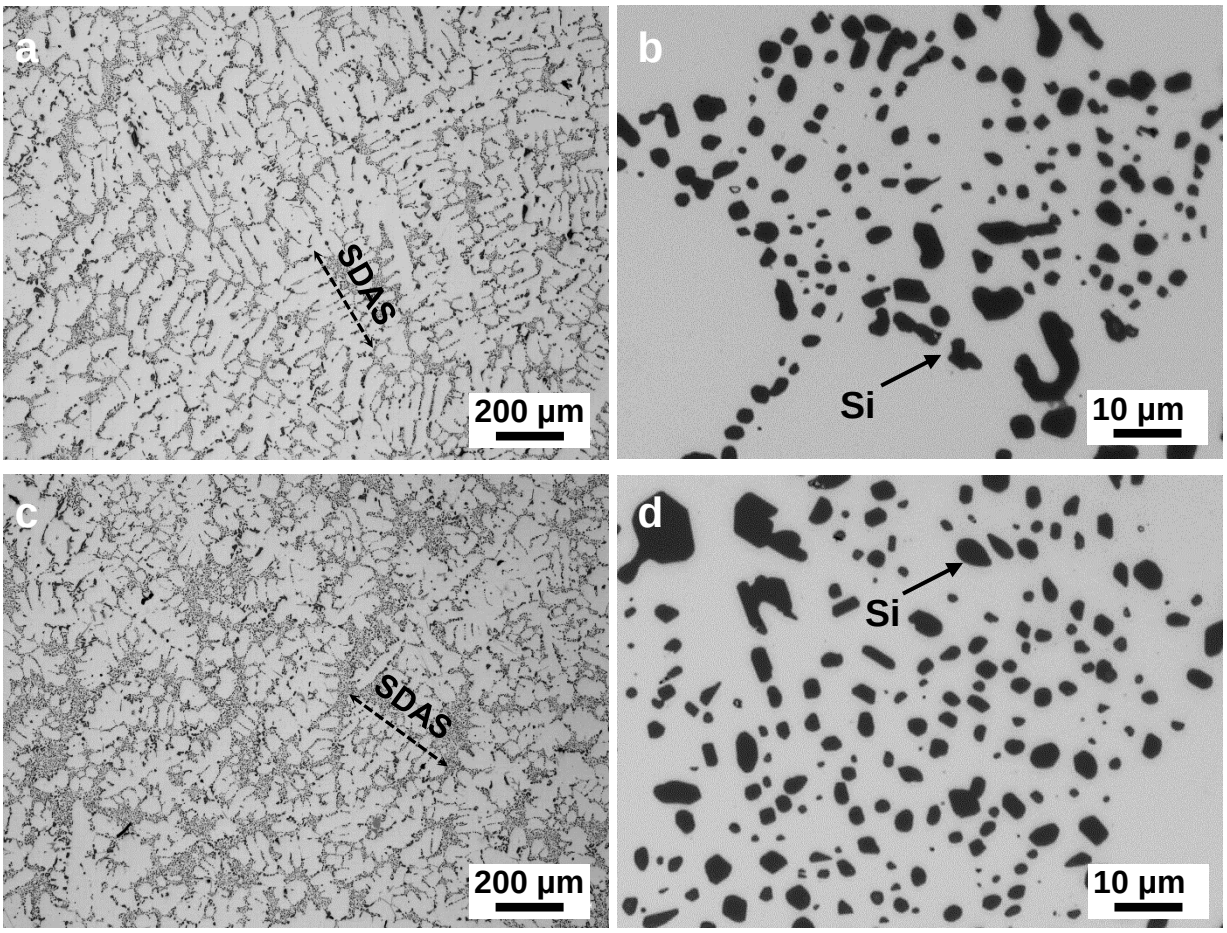

Figure 3 Optical micrographs showing the primary α-Al and eutectic Si phases of (a, b) baseline, and (c, d) Zr-modified Al-Si-Cu-Mg alloys after T6 heat treatment.

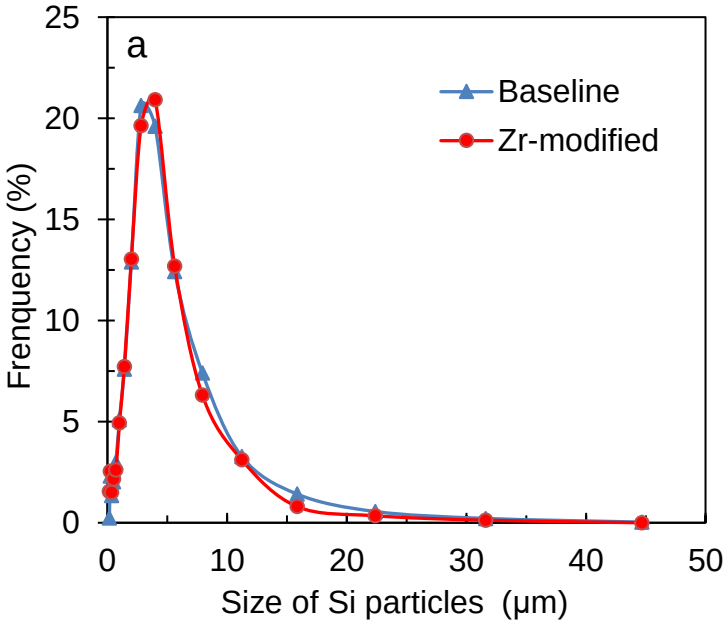

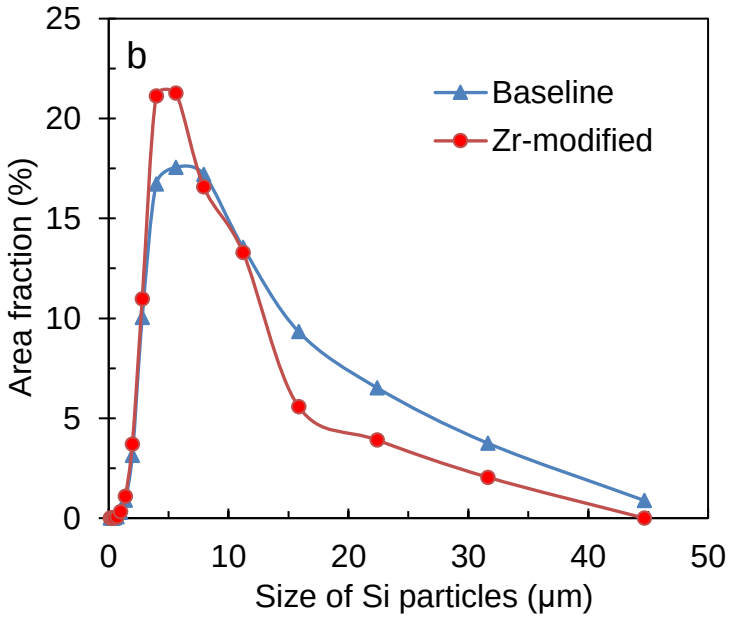

Figure 4 The size distribution of the Si particles of the baseline and Zr-modified Al-Si-Cu-Mg alloys after T6 heat treatment. (a) number fraction, and (b) area fraction. More than 10000 individual Si particles were statistically measured.

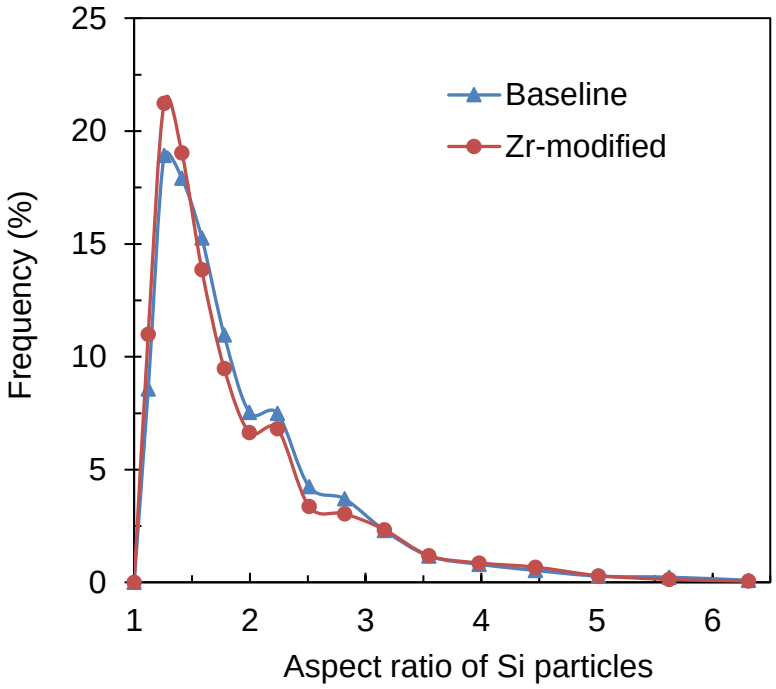

Figure 5 The aspect ratio distribution of the Si particles of the baseline and Zr-modified Al-Si-Cu-Mg alloys after T6 heat treatment. More than 10000 individual Si particles were statistically measured.

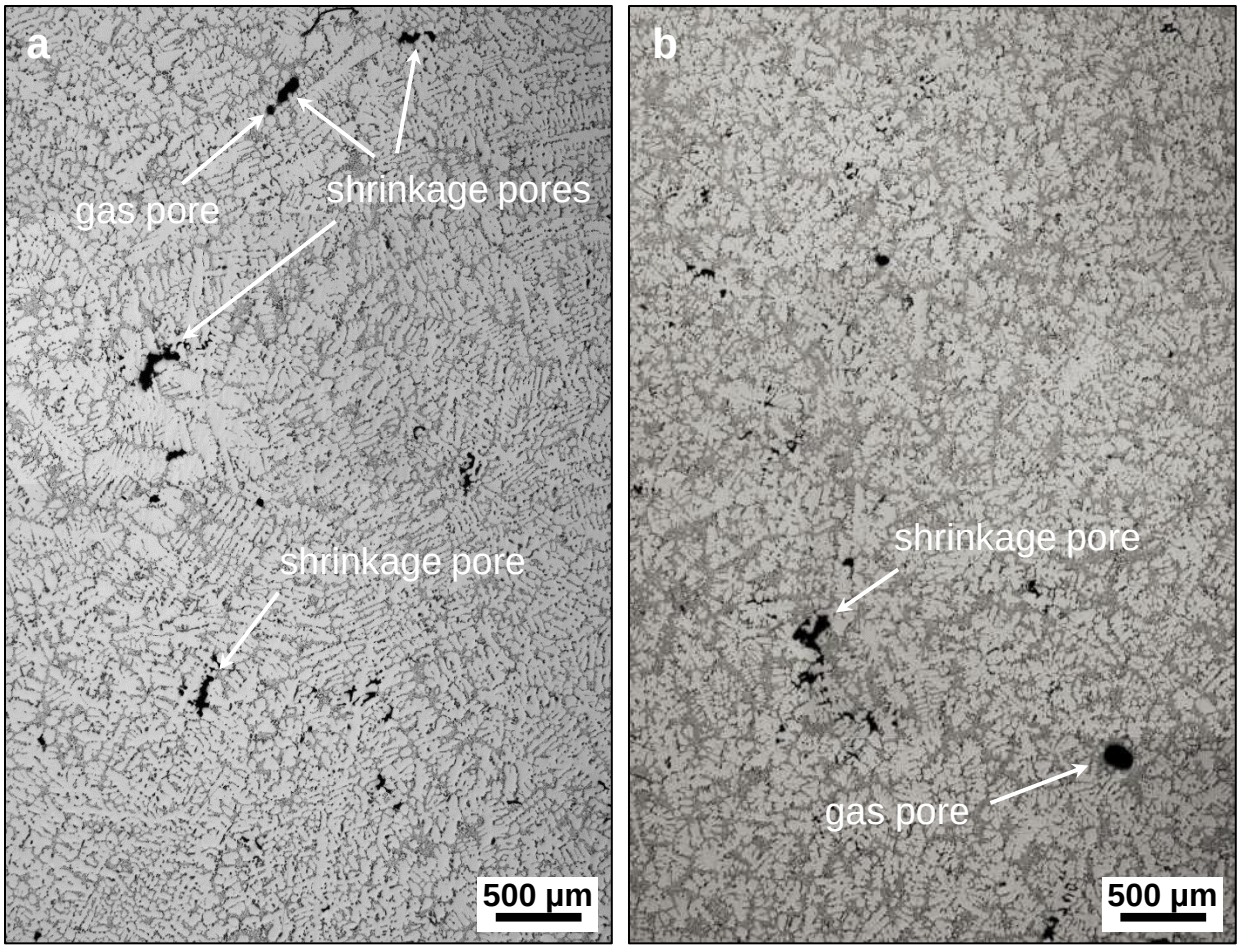

Figure 6 Optical micrographs showing the gas and shrinkage pores of (a) the baseline and (b) Zr-modified Al-Si-Cu-Mg alloys after T6 heat treatment.

Table 2 Comparison of the quantitative metallographic characteristics of α-Al, eutectics, Si particles, and porosities of the experimental Al-Si-Cu-Mg alloys. GS: Grain size, SDAS: Secondary dendrite arm spacing.

Alloys	**α-Al**		**Eutectics**	**Si particles**		**Porosities**		
	GS (μm)	SDAS (μm)	Area fraction (%)	Mean Ferret diameter (μm)	Mean aspect ratio	Area fraction (%)	Mean aspect ratio	Mean Ferret diameter (μm)
Baseline	335±18	39±2	27.9±1.2	3.3±1.9	1.65±0.44	0.33±0.02	2.4±0.1	110.2±11.2
Zr-modified	253±41	28±3	33.1±0.9	3.1±1.7	1.61±0.44	0.31±0.03	2.0±0.2	106.1±9.6

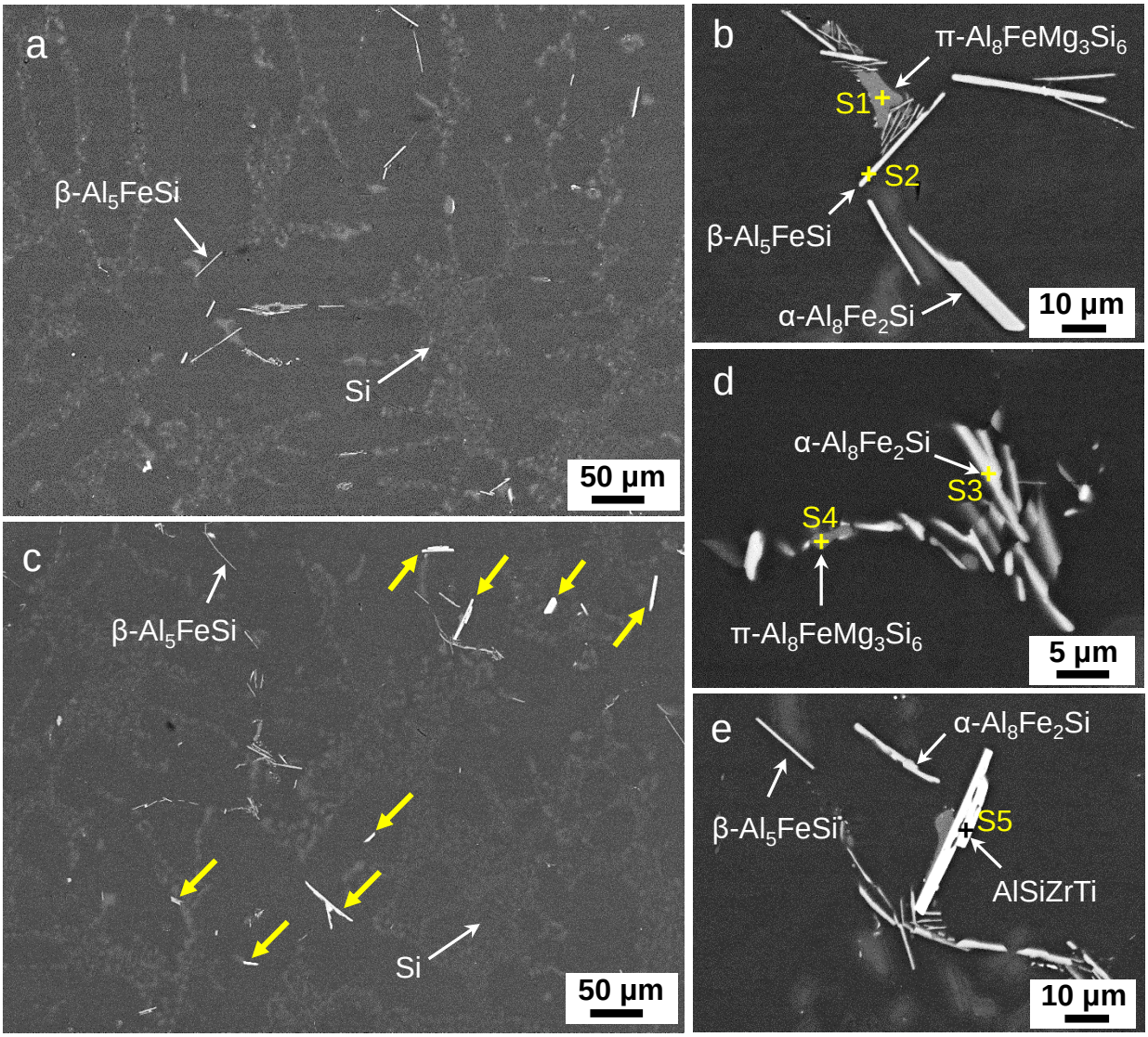

Figure 7 BSE-SEM micrographs showing the Fe-rich and Zr-containing intermetallic phases in the Al-Si-Cu-Mg alloys after T6 heat treatment: (a, b) baseline, and (c, d, e) Zr-modified.

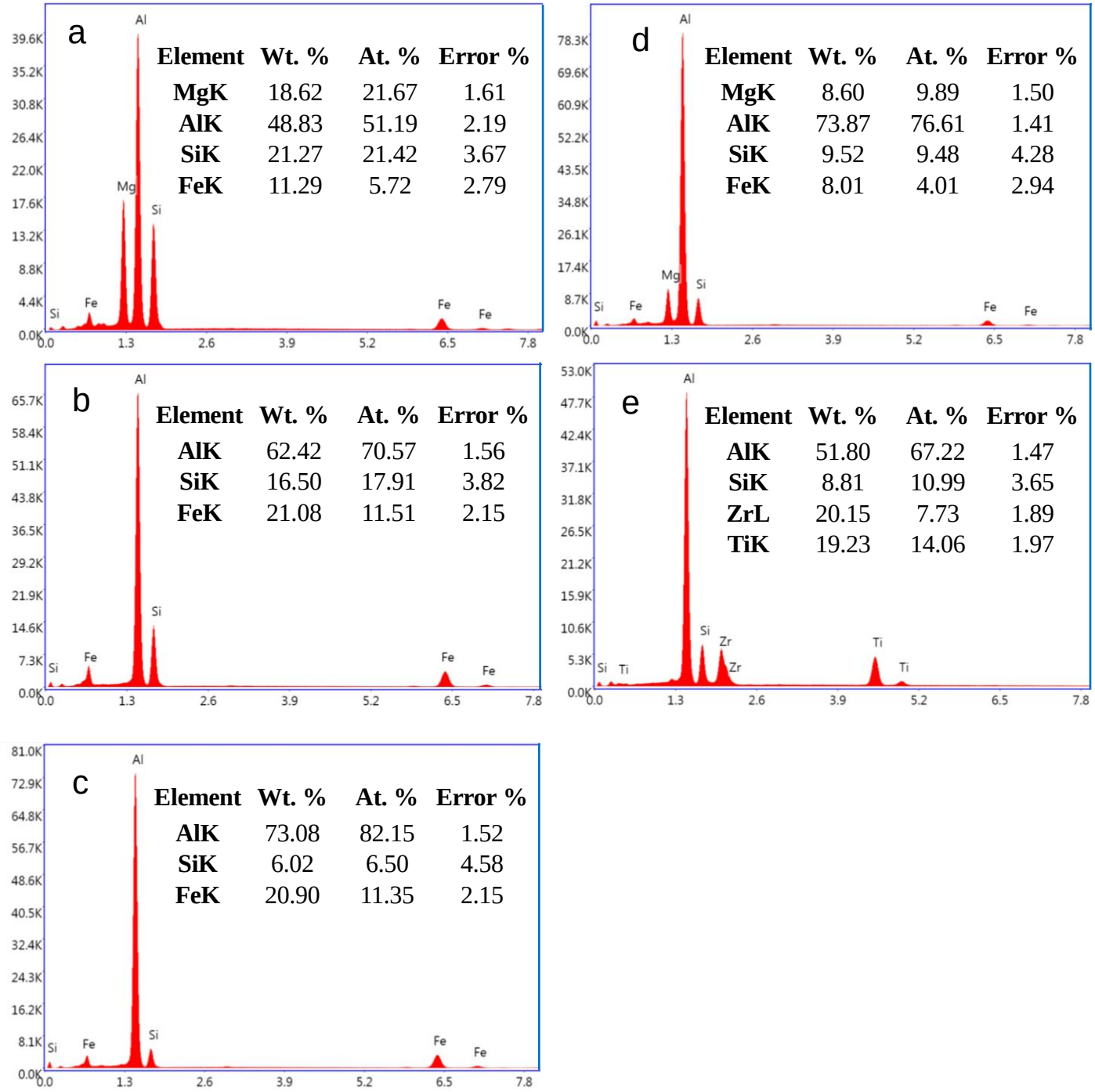

Figure 8 EDS analysis of the Fe-rich and Zr-containing intermetallic phases corresponding to the spectrums in Figure 7: (a) S1, (b)S2, (c) S3, (d) S4, and (e) S5.

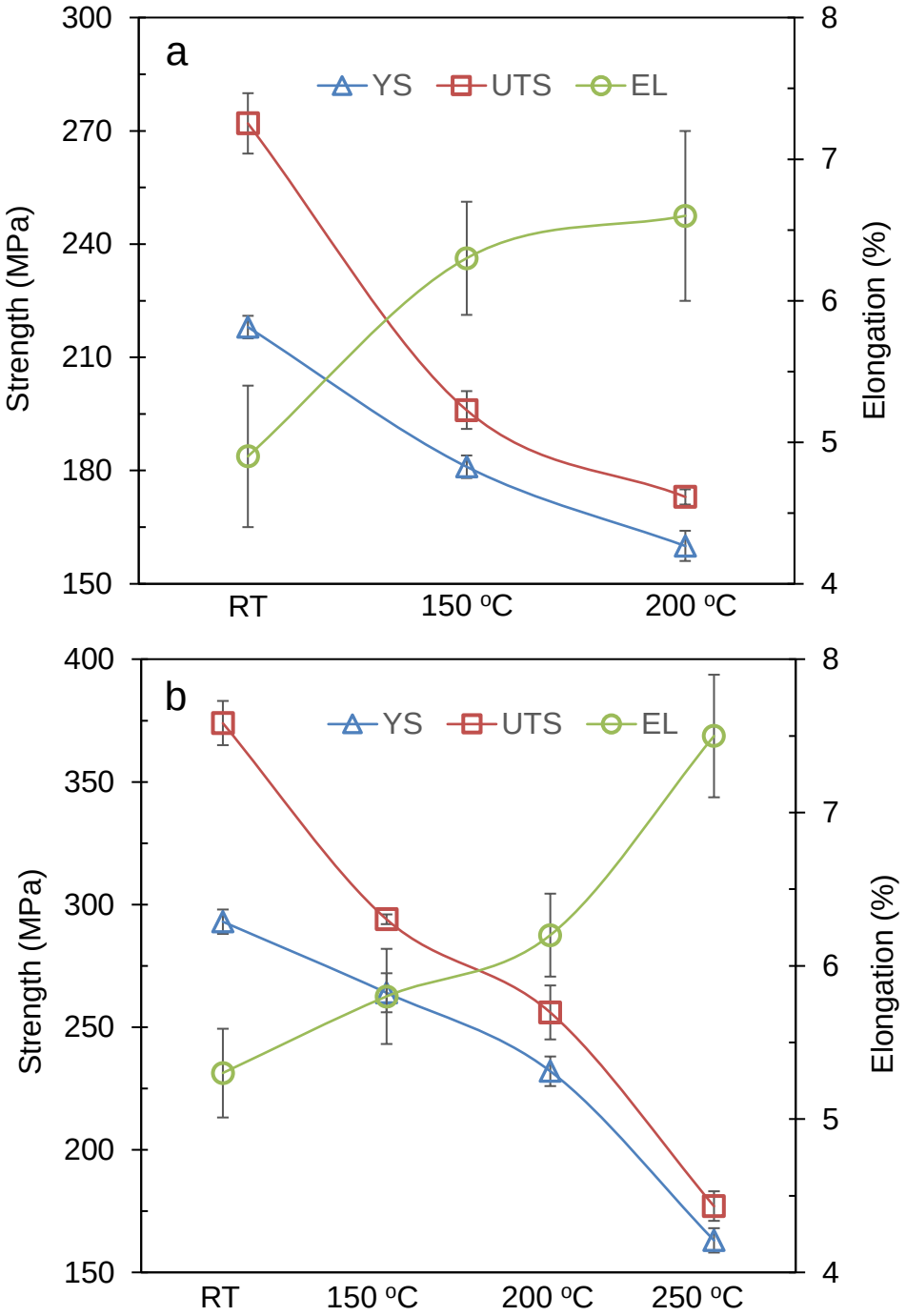

Figure 9 Tensile properties of (a) the baseline and (b) Zr-modified Al-Si-Mg-Cu alloys at different temperatures, RT: room temperature.

Table 3 The tensile properties of the baseline and Zr-modified Al-Si-Cu-Mg alloys tested at room and elevated temperatures.

Alloys	**Test conditions**	**YS (MPa)**	**UTS (MPa)**	**EL (%)**
Baseline	RT	218	272	4.9
	150 ^{o}C	181	196	6.3
	200 ^{o}C	160	173	6.6
Zr-modified	RT	293	374	5.3
	150 ^{o}C	264	294	5.8
	200 ^{o}C	232	256	6.2
	250 ^{o}C	163	177	7.5

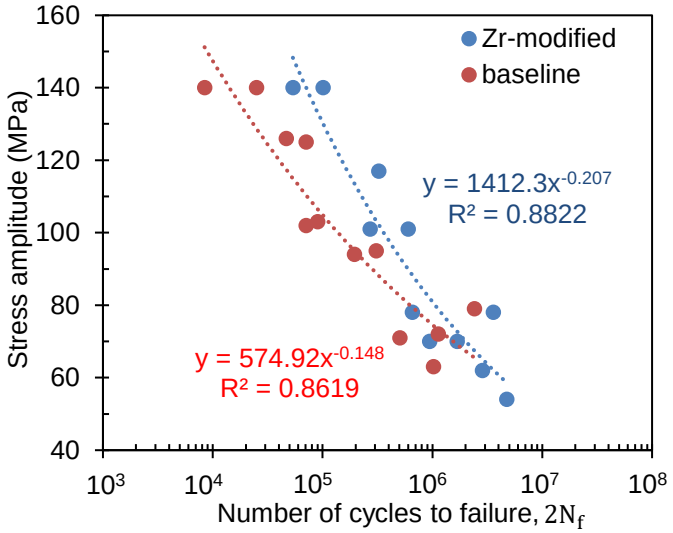

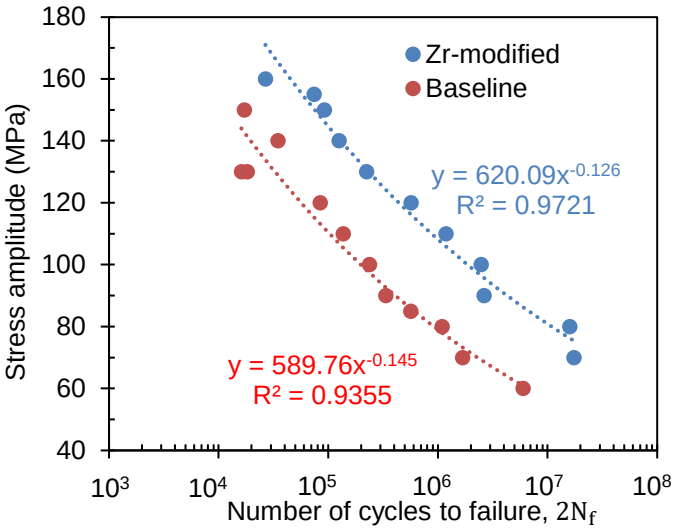

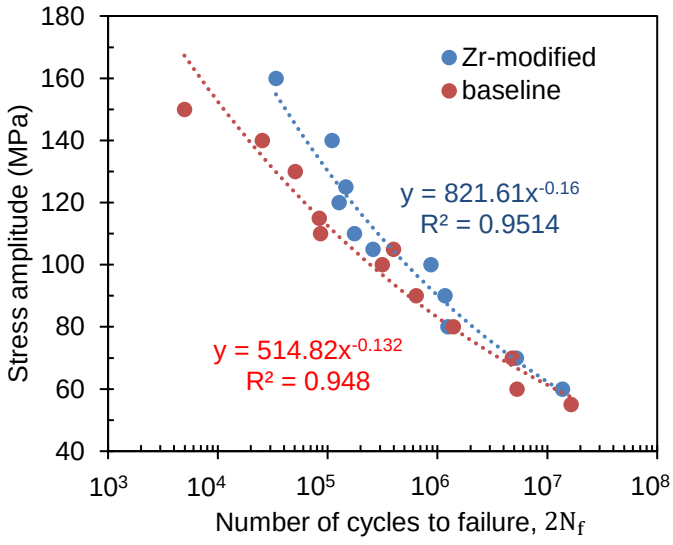

Figure 10 S-N curves of the baseline and Zr-modified Al-Si-Mg-Cu alloys tested at (a)150 ºC, (b) 200 ºC, and (c) 250 ºC.

Table 4 The fatigue strength coefficient ($\sigma_f{}'$) and fatigue strength exponent (b) of the baseline and Zr-modified Al-Si-Cu-Mg alloys tested at 150, 200, and 250 °C, $\sigma_a = \sigma_f{}' \ (2N_f)^b$.

Materials	150 °C			200 °C			250°C		
	$\sigma_f{}'$ (MPa)	b	R^2	$\sigma_f{}'$ (MPa)	b	R^2	$\sigma_f{}'$ (MPa)	b	R^2
Baseline	574.9	-0.148	0.841	589.8	-0.145	0.960	514.8	-0.132	0.960
Zr-modified	1412.3	-0.207	0.861	620.1	-0.126	0.973	821.6	-0.160	0.959

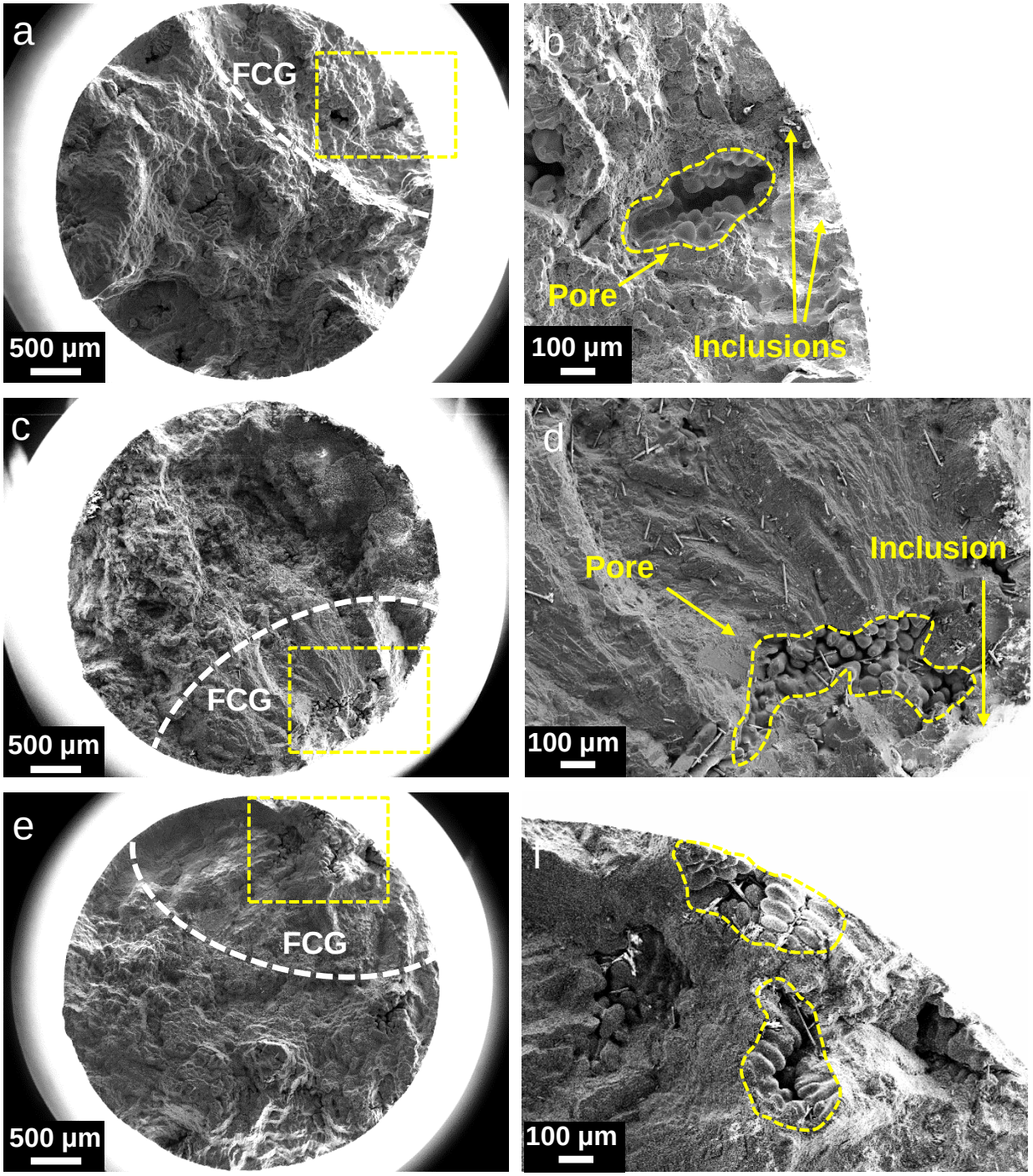

Figure 11 SEM micrographs showing the fatigue fracture surface of the baseline Al-Si-Cu-Mg alloys tested at 200 °C under different stress amplitudes of (a, b) 150 MPa, (c, d) 100 MPa, and (e, f) 70 MPa. FCG: Fatigue crack growth, FCI: Fatigue crack initiation.

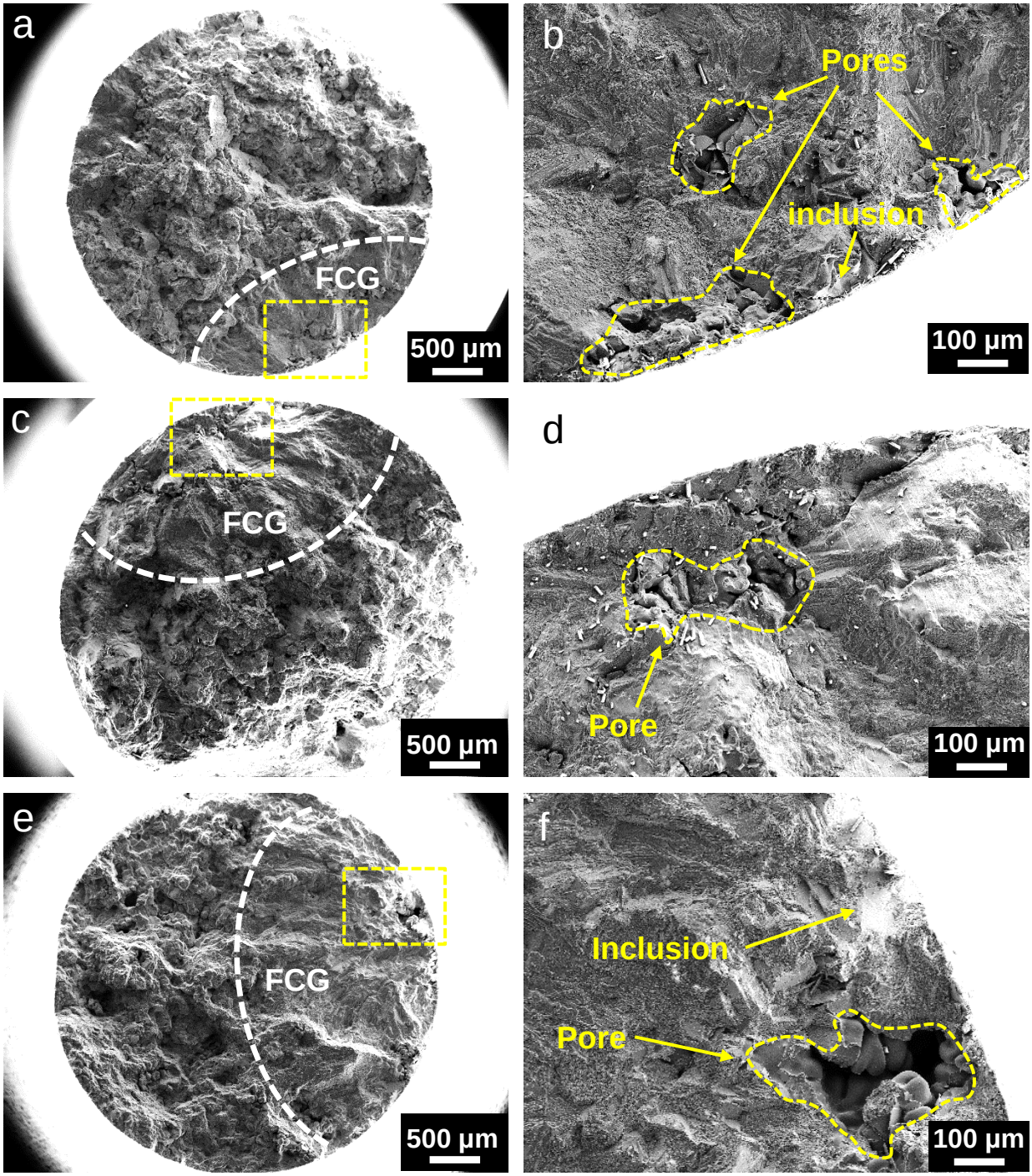

Figure 12 SEM micrographs showing the fatigue fracture surface of the Zr-modified Al-Si-Cu-Mg alloys tested at 200 °C under different stress amplitudes of (a, b) 150 MPa, (c, d) 100 MPa, and (e, f) 70 MPa. FCG: Fatigue crack growth, FCI: Fatigue crack initiation.

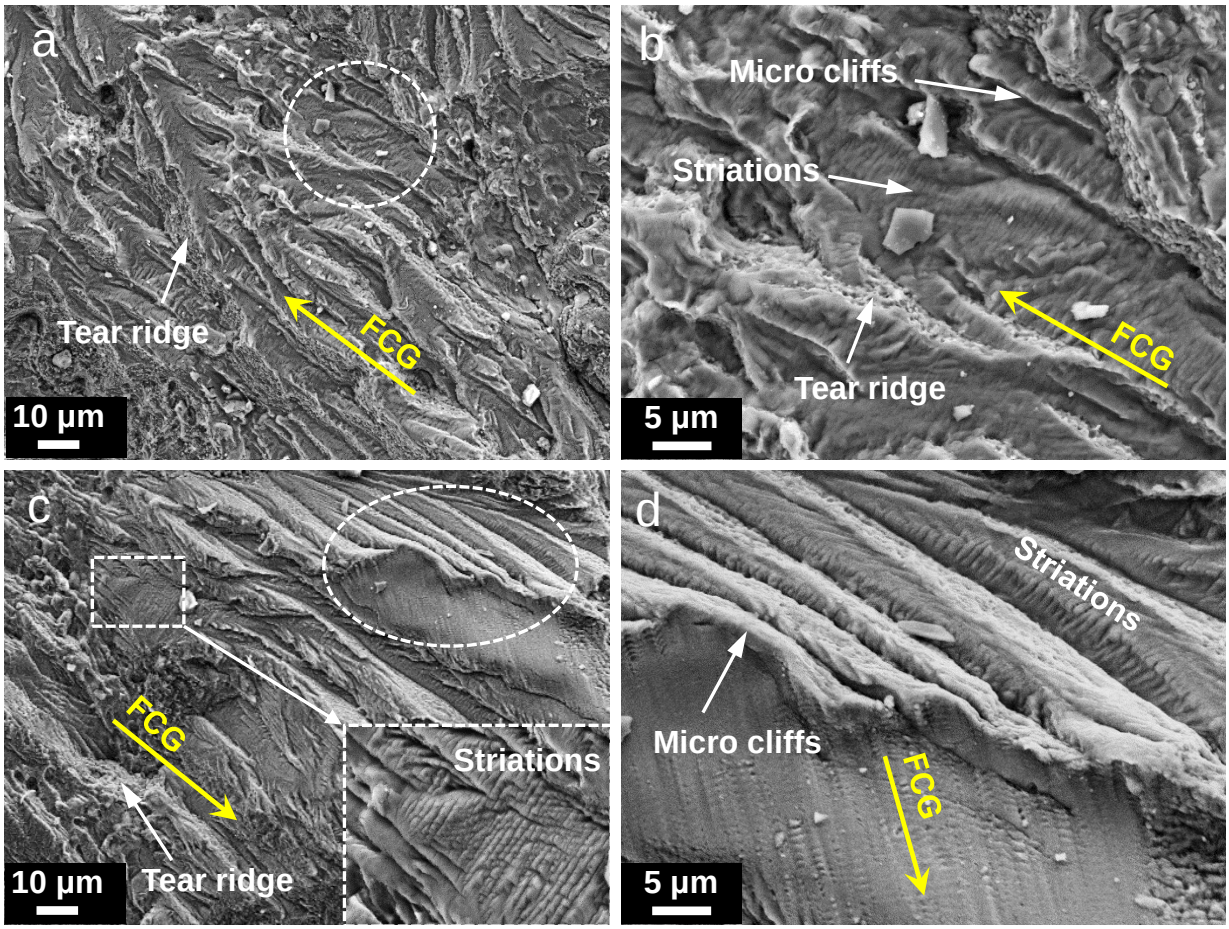

Figure 13 SEM micrographs of fatigue fracture surface, showing the fatigue crack growth of (a, b) the baseline and (c, d) Zr-modified Al-Si-Cu-Mg alloys tested at 200 ^{o}C under fatigue stress amplitudes of 100 MPa. FCG: Fatigue crack growth.

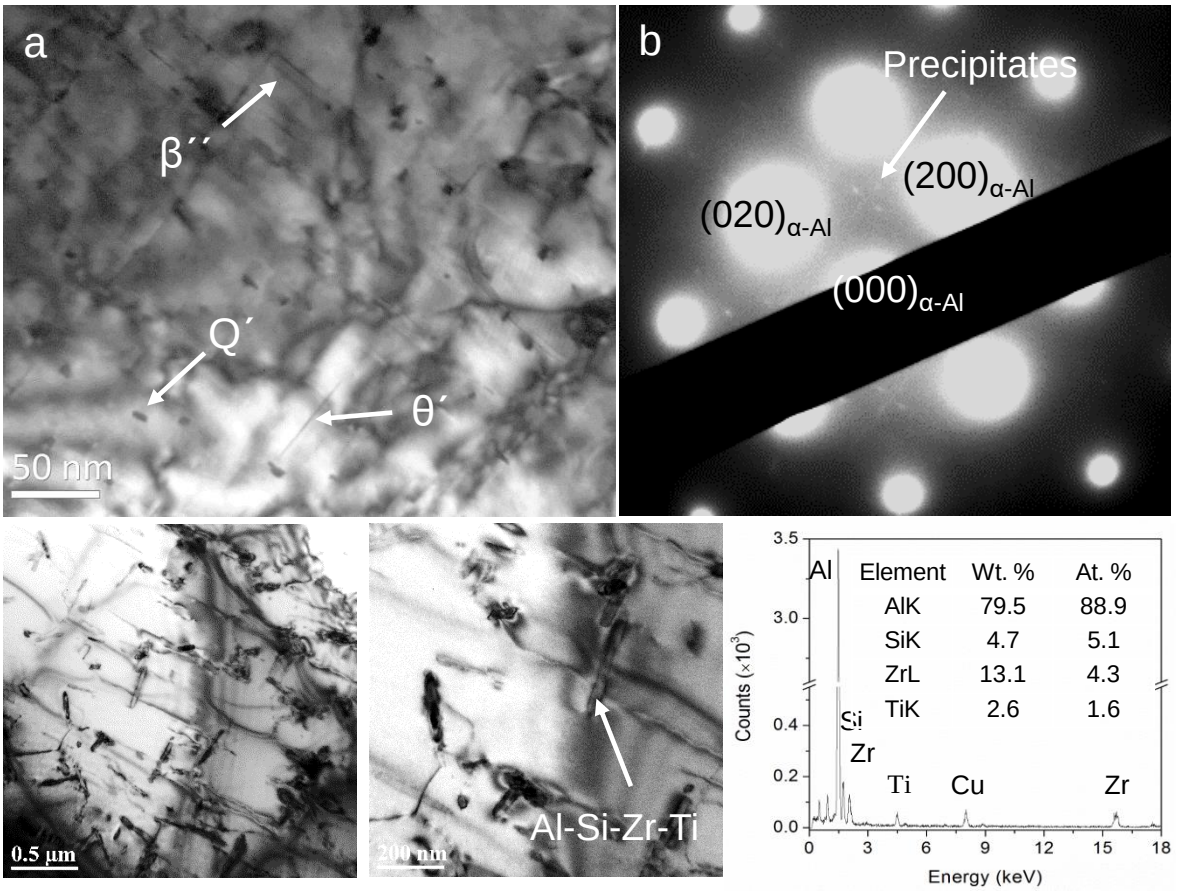

Figure 14 Bright-field TEM micrographs and EDS results, showing (a) the β´´, θ´, and Q´ precipitate phases and (b) corresponding SADP in the baseline Al-Si-Cu-Mg alloy; (c, d) the Al-Si-Zr-Ti precipitates in the Zr-modified Al-Si-Cu-Mg alloy, (e) the EDS results corresponding to the spectrum marked in (d).